Barriga, F.J.A.S., Binns, R.A., Miller, D.J., and Herzig, P.M. (Eds.)
Proceedings of the Ocean Drilling Program, Scientific Results Volume 193

8. Data Report: A Comprehensive Geochemical, Mineralogical, and Isotopic Data Set of Variably Altered Dacitic Volcanic Rocks from the Subsurface of the PACMANUS Hydrothermal Field (ODP Leg 193)[1]

H. Paulick,[2] P. Herzig,[3] and S. Hoernes[2]

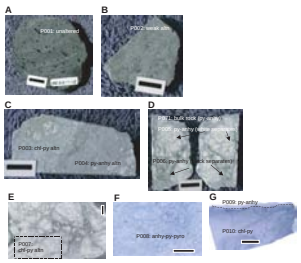

INTRODUCTION

A geochemical, mineralogical, and isotopic database comprising 75 analyses of Ocean Drilling Program (ODP) Leg 193 samples has been prepared, representing the variable dacitic volcanic facies and alteration types observed in drill core from the subsurface of the PACMANUS hydrothermal system (Table **T1**). The data set comprises major elements, trace and rare earth elements (REE), various volatiles (S, F, Cl, S, SO_4, CO_2, and H_2O), and analyses of $\delta^{18}O$ and $^{86}Sr/^{87}Sr$ for bulk rock and mineral separates (anhydrite). Furthermore, normative mineral proportions have been calculated based on the results of X-ray diffraction (XRD) analysis (Table **T2**) using the SOLVER function of the Microsoft Excel program.

Several of the samples analyzed consist of mesoscopically distinctive domains, and separate powders were generated to investigate these hand specimen–scale heterogeneities. Images of all the samples are collated in Figure **F1**, illustrating the location of each powder analyzed and documenting which measurements were performed.

[1]Paulick, H., Herzig, P., and Hoernes, S., 2005. Data report: A comprehensive geochemical, mineralogical, and isotopic data set of altered dacitic volcanic rocks from the subsurface of the PACMANUS hydrothermal field (ODP Leg 193). *In* Barriga, F.J.A.S., Binns, R.A., Miller, D.J., and Herzig, P.M. (Eds.), *Proc. ODP, Sci. Results,* 193, 1–18 [Online]. Available from World Wide Web: <http://www-odp.tamu.edu/publications/193_SR/VOLUME/CHAPTERS/209.PDF>. [Cited YYYY-MM-DD]
[2]Mineralogisch-Petrologisches Institut, Universität Bonn, Poppelsdorfer Schloss, 53115 Bonn, Germany. Correspondence author: **Holger.Paulick@uni-bonn.de**
[3]Lehrstuhl für Lagerstättenlehre und Leibniz-Labor für Angewandte Meeresforschung, Institut für Mineralogie, Bergakademie Freiberg, Brennhausgasse 14, 09596 Freiberg, Germany.

Initial receipt: 27 October 2003
Acceptance: 13 September 2004
Web publication: 5 April 2005
Ms 193SR-209

MATERIALS AND METHODS

Sample Treatment, Analytical Methods, and Data Quality

Many mixed-layer phyllosilicates become unstable at temperatures of ~100°C, resulting in phase transformation and loss of volatile components (mainly H_2O or OH) contained in the crystal lattice. Because mixed-layer phyllosilicates are prominent in the hydrothermally altered dacites from the PACMANUS system, the powders were dried at 80°C overnight prior to any analyses.

Major elements and some trace elements (Ba, Rb, Sr, Y, and Zr) were measured by X-ray fluorescence (XRF) using fused disks at the Mineralogisch-Petrologisches Institut (Universität Bonn, Germany). The internal standard powders from Holes 1188B and 1191A were included in three batches, and the results of these measurements on individual fused disks provide an indication of the reproducibility of the data (Table **T1**). The analyses were performed on a Philips PW1480 X-ray spectrometer using Oxiquant software and 85 international standards for calibration. The totals for major elements and volatiles range from 98.5 to 101.5 wt%. In this regard, it was important to take the appropriate concentrations of water-soluble SO_4 for anhydrite-rich samples into account.

Inductively coupled plasma–mass spectrometer (ICP-MS) measurements for Cu, Pb, Zn, Ba, Ag, As, Bi, Cd, Cr, Co, Ga, Mo, Ni, Rb, Sb, Sc, Sr, Tl, and U were performed on a PerkinElmer Elan 5000 instrument at the Institut für Mineralogie (Bergakademie Freiberg, Germany). Dissolution of the samples was achieved using concentrated HF and HNO_3 under atmospheric conditions. However, for some samples, this method was not sufficient to completely dissolve the zircon microcrystals, which led to deficiencies in Zr, Hf, Th, Y, and heavy rare earth elements (HREE). This could be clearly recognized by examining the REE patterns and comparing the Zr measurements by ICP-MS to the Zr concentrations determined by XRF. Consequently, additional ICP-MS data were obtained from the ICP-MS laboratories at the University of Kiel and at the GeoForschungsZentrum Potsdam (GFZ). At GFZ Potsdam, samples were dissolved using HF, $HClO_4$, and HCl in a multistage procedure that involved heating the samples at 180°C in pressurized Teflon vessels (Dulski, 2001). The solutions were analyzed with an Elan 5000A PerkinElmer Sciex instrument. At Kiel, glass beads were generated using ~250 mg of pulverized sample and lithium metaborate fusion. The beads were dissolved in HNO_3, and the solutions were analyzed with an Agilent 7500c ICP-MS instrument. Details of this procedure are documented in Garbe-Schönberg (1993). The analyses presented in Table **T1** have $Zr_{XRF}/Zr_{ICP\text{-}MS}$ ratios ranging from 0.8 to 1.2, which is an indication that the zircon microcrystals have been successfully dissolved and that the ICP-MS measurements of Zr, Hf, Th, Y, and HREE are accurate.

The H_2O concentration was determined by thermal dissociation and infrared quantitative flow analysis using a Rosemount gas analyzer at the GEOMAR Institute (Kiel, Germany). Again, all samples were dried at 80°C to prevent destruction of some secondary phyllosilicates. Hence, values for the unaltered samples may include some water related to incipient hydration of the glassy groundmass that was not expelled at this temperature.

Measurements of S, C, and N were performed by thermal dissociation and element analysis in a VARIO EL gas analyzer (Institut für Mineralogie, Bergakademie Freiberg, Germany). Accuracy and precision were ensured by analyses of several duplicates and internal laboratory standards. For samples with >1 wt% S_{total}, the content of water-soluble SO_4 was determined gravimetrically at the Institut für Mineralogie (Bergakademie Freiberg, Germany) in order to account for the anhydrite content of many hydrothermally altered samples. About 2 g of sample powder was washed in ~500 mL of cold, distilled H_2O for >12 hr. The dissolved SO_4 was reacted with BaCl, causing quantitative precipitation of $BaSO_4$, proportional to the concentration of the water-soluble sulfate in the sample. The detection limit is on the order of 0.6 wt% $CaSO_4$ in the sample, and repeated analyses show that the relative error of the measurements is on the order of 5%.

The concentrations of F and Cl were determined for several samples at the Institut für Mineralogie (Bergakademie Freiberg, Germany) following procedures outlined by Klemm (1980). In order to remove any salt crystals (halite) from the samples, the samples were washed in warm water (30°C) for >1 hr prior to measurement. These powders were reacted with ZnO and Na_2CO_3 at 900°C, which liberated F and Cl from the silicate phases. These powders were dissolved in distilled H_2O, and concentrations were determined using appropriate ion-selective electrodes. The detection limit was 200 ppm, and repeated analyses of particular samples indicate a relative error of 5% for F and Cl. A subset of seven samples was also analyzed for Cl at AnalytikJena AG (Germany) using a newly developed elemental analyzer (multi EA 2000), and these data are in agreement with our results (Table **T1**).

The $\delta^{18}O_{silicate}$ relative to the Vienna standard mean ocean water (VSMOW) was determined for 38 samples at the Mineralogisch-Petrologisches Institut (Universität Bonn, Germany). Where present, anhydrite was removed from the powders prior to analysis and the oxygen was liberated in a standard fluorination line using ultrapure F_2 gas reacting with the sample powder at 600°C in Ni ovens. The liberated oxygen was transformed to CO_2, and the $\delta^{18}O_{silicate}$ was measured with a SIRA-9 mass spectrometer. At least two individual $\delta^{18}O_{silicate}$ determinations were performed, and the average of these measurements is reported in Table **T1.** Deviation from the average is generally less than ±0.1‰, but in some cases it is up to ±0.2‰.

The $\delta^{18}O_{anhydrite}$ was determined for 24 samples using the $BaSO_4$ powder generated during the gravimetric determination of water-soluble SO_4. A method based on thermal combustion and online $\delta^{18}O$ measurement was applied at the Institut für Mineralogie (Bergakademie Freiberg, Germany) following procedures described by Kornexl et al. (1999). National Bureau of Standards (NBS) 127 reference material ($BaSO_4$) was used for calibration of this method, and repeated analyses show that the reproducibility is generally ±0.3‰.

The $^{86}Sr/^{87}Sr_{silicate}$ ratio was determined for 49 samples at the Institut für Mineralogie (Bergakademie Freiberg, Germany). Where present, anhydrite was removed to generate powders consisting exclusively of silicates. In addition, the $^{86}Sr/^{87}Sr_{anhydrite}$ ratio was measured for 24 samples that contain significant amounts of anhydrite (>1 wt% water-soluble SO_4). The anhydrite was dissolved from the powders by washing in cold, distilled water for >12 hr. The measured $^{86}Sr/^{87}Sr$ ratio of the solutions is equal to the $^{86}Sr/^{87}Sr_{anhydrite}$ of the samples. All measurements

were performed with a Finnigan MAT 263 mass spectrometer. Repeated analyses of $^{86}Sr/^{87}Sr_{silicate}$ for individual samples were in excellent agreement and within the range of the error of the measurements (0.00001 to 0.00005). NBS 127 reference material was used to ensure accuracy of the measurements. Based on one duplicate analysis, the reproducibility of $^{86}Sr/^{87}Sr_{anhydrite}$ appears to be somewhat poorer (±0.0002), which could be related to problems during dissolution of the anhydrite from the sample powder.

The results of the mineral phase analysis by XRD are presented in Table T2. Step-scan XRD measurements (3°2θ–80°2θ; 0.03°2θ step size; and 5 s/step) were collected on spun samples with an RD 7 diffractometer (Seifert-FPM) at the Institut für Mineralogie (Bergakademie Freiberg, Germany). The diffractometer was equipped with a diffracted beam graphite monochromator and a variable divergence slit that allowed the irradiation of a constant sample area. A CuK_α tube was used and operated at 40 kV and 40 mA. Qualitative phase analysis of the diffraction pattern was carried out by conventional search/match procedures using reference diffraction patterns stored in the International Centre for Diffraction Data (ICDD) PDF-2.

Using the results of the XRD analyses and the major element data, it was possible to run iterative calculations using the SOLVER function in an Excel spreadsheet to calculate normative mineral abundances. Based on assumed chemical compositions of the detected mineral phases, this calculation optimizes the proportions of the minerals until the calculated bulk rock composition is closest to the measured bulk rock composition. The results of these procedures are presented in Table T1.

RESULTS

Compositional Variations Determined from Normative Mineral Assemblages

Based on the compositional variations observed in the data set, the samples were divided into six different groups: unaltered dacite, weakly altered dacite, chlorite-pyrite alteration, K-feldspar-illite alteration, anhydrite-pyrite-pyrophyllite alteration, and pyrite-anhydrite alteration (Fig. F2). However, it should be stressed that the alteration at PACMANUS represents a continuous spectrum and there is a significant degree of overlap between some of the groups defined. Nevertheless, the groups reflect different stages during the geochemical and mineralogical changes associated with hydrothermal water/rock interaction. These are characterized by destruction of primary mineral phases such as plagioclase and formation of various hydrothermal phyllosilicates (chlorite, illite, pyrophyllite, paragonite, and mixed-layer clays), pyrite, anhydrite, and hydrothermal K-feldspar.

Unaltered dacite commonly has a glassy matrix, and normative anorthite and albite are dominant. They contain some normative K-feldspar and very minor normative chlorite-smectite. The weakly altered samples are still dominated by normative feldspar, but hydrothermal phyllosilicates are somewhat more abundant. Pyrite and anhydrite are virtually absent in these two groups.

The K-feldspar-illite alteration is characterized by decreased normative anorthite + albite concentrations and elevated concentrations of hydrothermal K-feldspar and illite. However, there is considerable heterogeneity in this group and some samples have normative anorthite +

F2. Normative abundances of the most important minerals, p. 14.

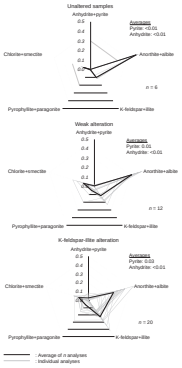

albite concentrations comparable to weakly altered samples, whereas others contain significant pyrite.

The concentrations of hydrothermal chlorite and smectite are particularly elevated in the chlorite-pyrite alteration. Again, there is some compositional heterogeneity in this group; however, the concentration of anorthite and albite are lower on average than in the K-feldspar-illite alteration. Most samples contain appreciable amounts of pyrite and/or anhydrite.

Samples of the anhydrite-pyrite-pyrophyllite alteration and the pyrite-anhydrite alteration are the most strongly altered in the PACMANUS hydrothermal system and contain little or no plagioclase. They contain significant illite, as well as pyrophyllite and/or paragonite and minor chlorite and smectite. The anhydrite-pyrite-pyrophyllite alteration is characterized by the predominance of anhydrite compared to pyrite, whereas the pyrite-anhydrite alteration is pyrite rich.

Most of the samples were collected from drill holes at the Snowcap (Holes 1188A and 1188F) and the Roman Ruins (Holes 1189A and 1189B) hydrothermal sites. There are some systematic differences in the composition of altered dacite between these two sites (Fig. F3). Most samples from Roman Ruins contain >10 wt% normative K-feldspar, whereas samples from Snowcap generally contain <5 wt% normative K-feldspar (average = 3 wt%). In contrast, samples from Roman Ruins contain no or minor normative pyrophyllite + paragonite (<10 wt%), whereas altered dacite from Snowcap generally shows elevated concentrations in normative pyrophyllite and paragonite with a fairly even spread between 5 and 35 wt%. These compositional characteristics point to substantial differences in the hydrothermal regime between these two sites and may be related to distinctive hydrothermal fluids.

F3. Hydrothermal minerals in altered dacite, p. 16.

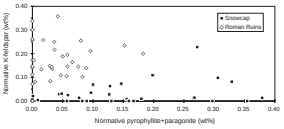

ACKNOWLEDGMENTS

The authors would like to thank Professor Klemm, Ms. Rüdiger, Mr. Gabriel, and Ms. Bombach for analyses at the geochemistry laboratory of the Institut für Mineralogie (Bergakademie Freiberg, Germany). The Sr-isotopic compositions and $\delta^{18}O_{anhydrite}$ were determined by Dr. Tichomirowa and Ms. Liebscher, and the XRD data were generated with the help of Dr. Kleeberg and Ms. Köhler. The H_2O analyses were performed by Ms. Rau at GEOMAR (Kiel, Germany). Dr. Hoffbauer and Ms. Dohle assisted with XRF and $\delta^{18}O_{silicate}$ measurements at the Mineralogisch-Petrologisches Institut (Universität Bonn, Germany). Dr. Bach (Woods Hole Oceanographic Institution) developed the Excel spreadsheet for calculation of normative mineral abundances. This research used data and samples supplied by the Ocean Drilling Program (ODP). ODP is sponsored by the U.S. National Science Foundation (NSF) and participating countries under management of Joint Oceanographic Institutions (JOI), Inc.

REFERENCES

Dulski, P., 2001. Reference materials for geochemical studies: new analytical data by ICP-MS and critical discussion of reference values. *Geostand. Newsl.,* 25:87–125.

Garbe-Schönberg, C.-D., 1993. Simultaneous determination of thirty-seven trace elements in twenty-eight international rock standards by ICP-MS. *Geostand. Newsl.,* 17:81–97.

Kornexl, B.E., Gehre, M., Höfling, R, and Werner, R.A., 1999. On-line $\delta^{18}O$ measurement of organic and inorganic substances. *Rapid Commun. Mass Spectrom.,* 13:1685–1693.

Klemm, W., 1980. Erfahrungen beim Einsatz der LaF3-Einkristallmembran-elektrode zur Fluorbestimmung in Silikaten. *Z. Angew. Geol.,* 26:561–565.

Figure F1. Images of ODP core samples analyzed from the subsurface of the PACMANUS hydrothermal field. Many samples consist of compositionally distinctive domains, and separate powders were generated for geochemical, mineralogical, and isotopic analyses. Here, the hand specimen expression of particular volcanic and alteration features are documented and the location of the analyzed powders are shown. In total, 75 powders derived from 54 samples were analyzed. The data are presented in Tables T1, p. 17, and T2, p. 18. Scale bar = 1 cm. altn = alteration, anhy =anhydrite, chl = chlorite, ill = illite, Kfsp = K-feldspar, py = pyrite, pyro = pyrophyllite. XRF = X-ray fluorescence, ICP-MS = inductively coupled plasma–mass spectrometry. **A.** Sample PM01 (193-1188A-2R-1, 18 cm): fresh, glassy, vesicular dacite. Bulk rock powder: P001 (XRF, ICP-MS, F, Cl, $\delta^{18}O_{silicate}$, $^{86}Sr/^{87}Sr_{silicate}$). **B.** Sample PM02 (193-1188A-5R-1, 37 cm): weakly altered, perlitic dacite. Bulk rock powder: P002 (XRF, ICP-MS, F, Cl, $\delta^{18}O_{silicate}$, $^{86}Sr/^{87}Sr_{silicate}$). **C.** Sample PM05 (193-1188A-7R-1, 114 cm): domainal altered dacite with remnant perlite. Powder of separates: P003 (XRF, ICP-MS, $\delta^{18}O_{anhydrite+silicate}$, $^{86}Sr/^{87}Sr_{anhydrite+silicate}$) and P004 (XRF, ICP-MS, $\delta^{18}O_{anhydrite+silicate}$, $^{86}Sr/^{87}Sr_{anhydrite+silicate}$). **D.** Sample PM06 (193-1188A-8R-1, 13 cm): domainal altered dacite with remnant perlite. Powders: P071 (bulk sample: XRF, ICP-MS, F, Cl), P005 (white domains: XRF, ICP-MS, $\delta^{18}O_{silicate}$, $^{86}Sr/^{87}Sr_{silicate}$), and P006 (black network: ICP-MS, $\delta^{18}O_{silicate}$,$^{86}Sr/^{87}Sr_{silicate}$). **E.** Sample PM07 (193-1188A-8R-1, 66 cm): light gray-green flow-banded, brecciated dacite. Bulk rock powder: P007 (XRF, ICP-MS, F, Cl, $\delta^{18}O_{anhydrite+silicate}$, $^{86}Sr/^{87}Sr_{anhydrite+silicate}$). **F.** Sample PM08 (193-1188A-8R-1, 13 cm): white ?perlitic, bleached coherent dacite. Bulk rock powder: P008 (XRF, ICP-MS, $\delta^{18}O_{anhydrite+silicate}$, $^{86}Sr/^{87}Sr_{anhydrite+silicate}$). **G.** Sample PM10 (193-1188A-11R-1, 20 cm): coherent dacite, gray kernel, and white margin. Powders: P009 (margin: XRF, ICP-MS, $\delta^{18}O_{anhydrite+silicate}$, $^{86}Sr/^{87}Sr_{anhydrite+silicate}$) and P010 (core: XRF, ICP-MS). (Continued on the next six pages.)

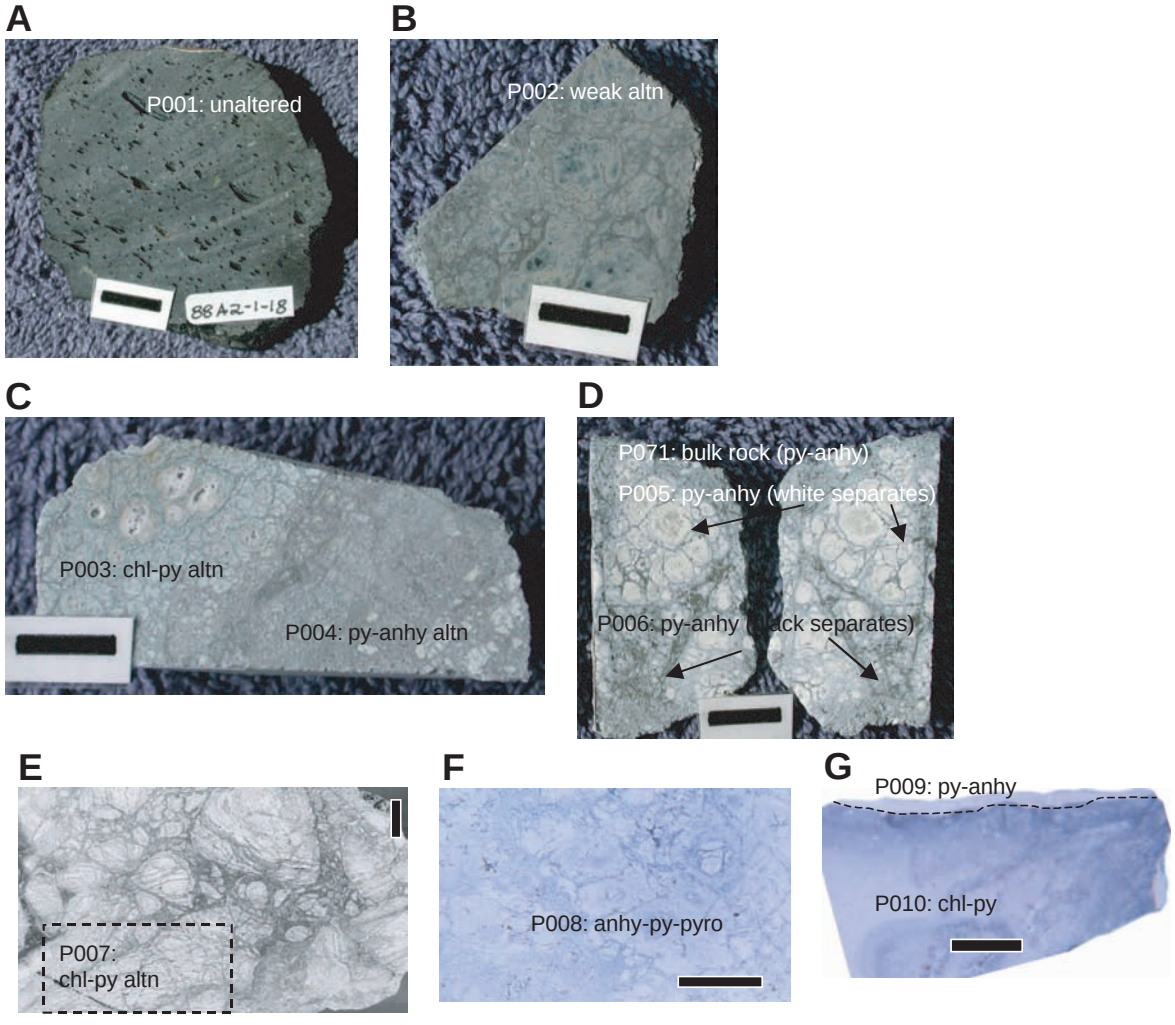

Figure F1 (continued). H. Sample PM11 (193-1188A-12R-2, 47 cm): gray-green flow-banded coherent dacite. Powder of separates: P011 (light gray: XRF, ICP-MS, F, Cl, $\delta^{18}O_{silicate}$, $^{86}Sr/^{87}Sr_{silicate}$) and P069 (dark gray: XRF, ICP-MS, F, Cl). **I.** Sample PM14 (193-1188A-14R-1, 86 cm): white, pseudoclastic, intensely veined coherent dacite. Powders: P012 (bulk rock: XRF, ICP-MS, $\delta^{18}O_{anhydrite + silicate}$, $^{86}Sr/^{87}Sr_{anhydrite + silicate}$) and P070 (separate of white kernels: XRF, ICP-MS). **J.** Sample PM15 (193-1188A-14R-1, 107 cm): volcanic breccia. Powders of separates: P014 (matrix: XRF, ICP-MS, $\delta^{18}O_{anhydrite + silicate}$, $^{86}Sr/^{87}Sr_{anhydrite + silicate}$) and P013 (clast: ICP-MS). **K.** Sample PM18 (193-1188A-17R-1, 24 cm): coherent dacite. Bulk rock powder: P015 (XRF, ICP-MS, F, Cl, $\delta^{18}O_{anhydrite + silicate}$, $^{86}Sr/^{87}Sr_{anhydrite + silicate}$). **L.** Sample PM20 (193-1188A-19R-1, 41 cm): amygdaloidal coherent dacite. Bulk rock powder: P016 (XRF, ICP-MS). **M.** Sample PM21 (193-1188A-19R-1, 86 cm): weakly altered vesicular, coherent dacite. Bulk rock powder: P017 (XRF, ICP-MS, F, Cl). **N.** Sample PM23 (193-1188A-20R-1, 95 cm): spherulitic coherent dacite. Powders of separates: P018 (spherulite-rich: XRF, ICP-MS, Cl, F, $\delta^{18}O_{silicate}$ + $^{86}Sr/^{87}Sr_{silicate}$) and P019 (spherulite-poor: XRF, ICP-MS, $\delta^{18}O_{anhydrite + silicate}$, $^{86}Sr/^{87}Sr_{anhydrite + silicate}$). **O.** Sample PM26 (193-1188F-6Z-1, 45 cm): weakly altered, spherulitic coherent dacite. Bulk rock powder: P020 (XRF, ICP-MS, $\delta^{18}O_{silicate}$, $^{86}Sr/^{87}Sr_{silicate}$).

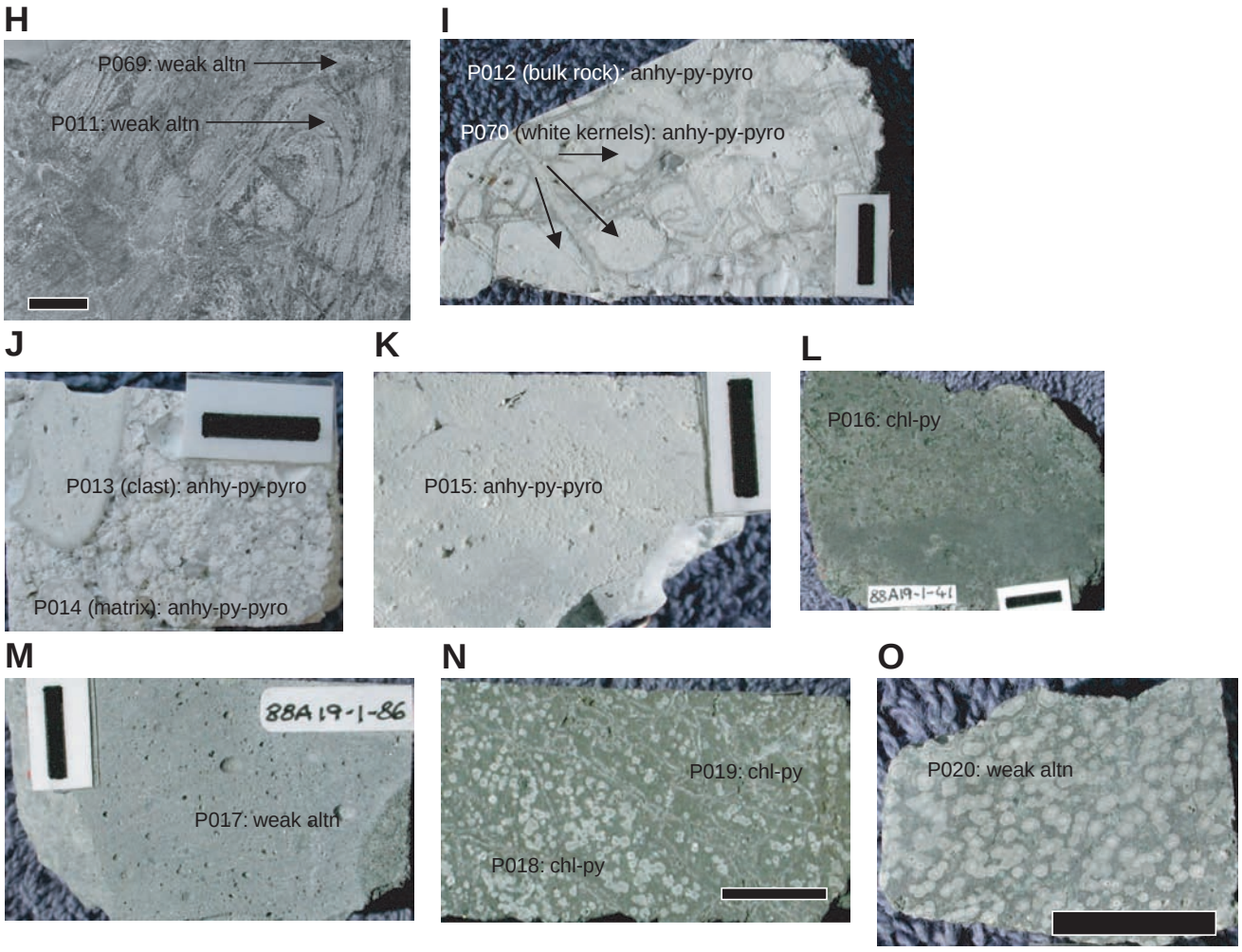

Figure F1 (continued). **P.** Sample PM27 (193-1188F-8Z-1, 26 cm): amygdaloidal coherent dacite. Powder of central part (excluding vein): P021 (XRF, ICP-MS, Cl, F, $\delta^{18}O_{anhydrite+silicate}$, $^{86}Sr/^{87}S_{anhydrite+silicate}$). **Q.** Sample PM29 (193-1188F-13Z-1, 0 cm): amygdaloidal coherent dacite, gray kernel, and white margin. Powders: P022 (margin: XRF, ICP-MS, $\delta^{18}O_{anhydrite+silicate}$, $^{86}Sr/^{87}Sr_{anhydrite+silicate}$) and P023 (kernel: XRF, ICP-MS, Cl, F, $\delta^{18}O_{anhydrite+silicate}$, $^{86}Sr/^{87}Sr_{anhydrite+silicate}$). **R.** Sample PM33 (193-1188F-19Z-1, 27cm): coherent dacite. Bulk rock powder: P024 (XRF, ICP-MS, Cl, F, $\delta^{18}O_{anhydrite+silicate}$, $^{86}Sr/^{87}Sr_{anhydrite+silicate}$). **S.** Sample PM35 (193-1188F-23Z-2, 56 cm): amygdaloidal coherent dacite, gray-green kernel, and yellow margin. Powders: P025 (kernel: XRF, ICP-MS, Cl, F, $\delta^{18}O_{silicate}$, $^{86}Sr/^{87}Sr_{silicate}$) and P026 (margin, excluding vein: XRF, ICP-MS, Cl, F, $\delta^{18}O_{silicate}$, $^{86}Sr/^{87}Sr_{silicate}$). **T.** Sample PM36 (193-1188F-30Z-1, 30 cm): volcaniclastic breccia. Bulk rock powder: P027 (XRF, ICP-MS). **U.** Sample PM37 (193-1188F-34Z-1, 123 cm): volcaniclastic? breccia. Bulk rock powder: P028 (XRF, ICP-MS, Cl, F). **V.** Sample PM40 (193-1188F-39Z-1, 82 cm): amygdaloidal coherent dacite. Bulk rock powder: P029 (XRF, ICP-MS, Cl, F, $\delta^{18}O_{anhydrite+silicate}$, $^{86}Sr/^{87}Sr_{anhydrite+silicate}$). **W.** Sample PM42 (193-1188F-43Z-1, 21 cm): amygdaloidal coherent dacite, gray-green kernel, and gray margin. Powders: P030 (kernel: XRF, ICP-MS, Cl, F, $\delta^{18}O_{anhydrite+silicate}$, $^{86}Sr/^{87}Sr_{anhydrite+silicate}$) and P031 (margin: XRF, ICP-MS, $\delta^{18}O_{anhydrite+silicate}$, $^{86}Sr/^{87}Sr_{anhydrite+silicate}$). **X.** Sample PM44 (193-1189A-1R-1, 12 cm): unaltered coherent aphyric dacite. Bulk rock powder: P032 (XRF, ICP-MS, Cl, F, $\delta^{18}O_{silicate}$, $^{86}Sr/^{87}Sr_{silicate}$).

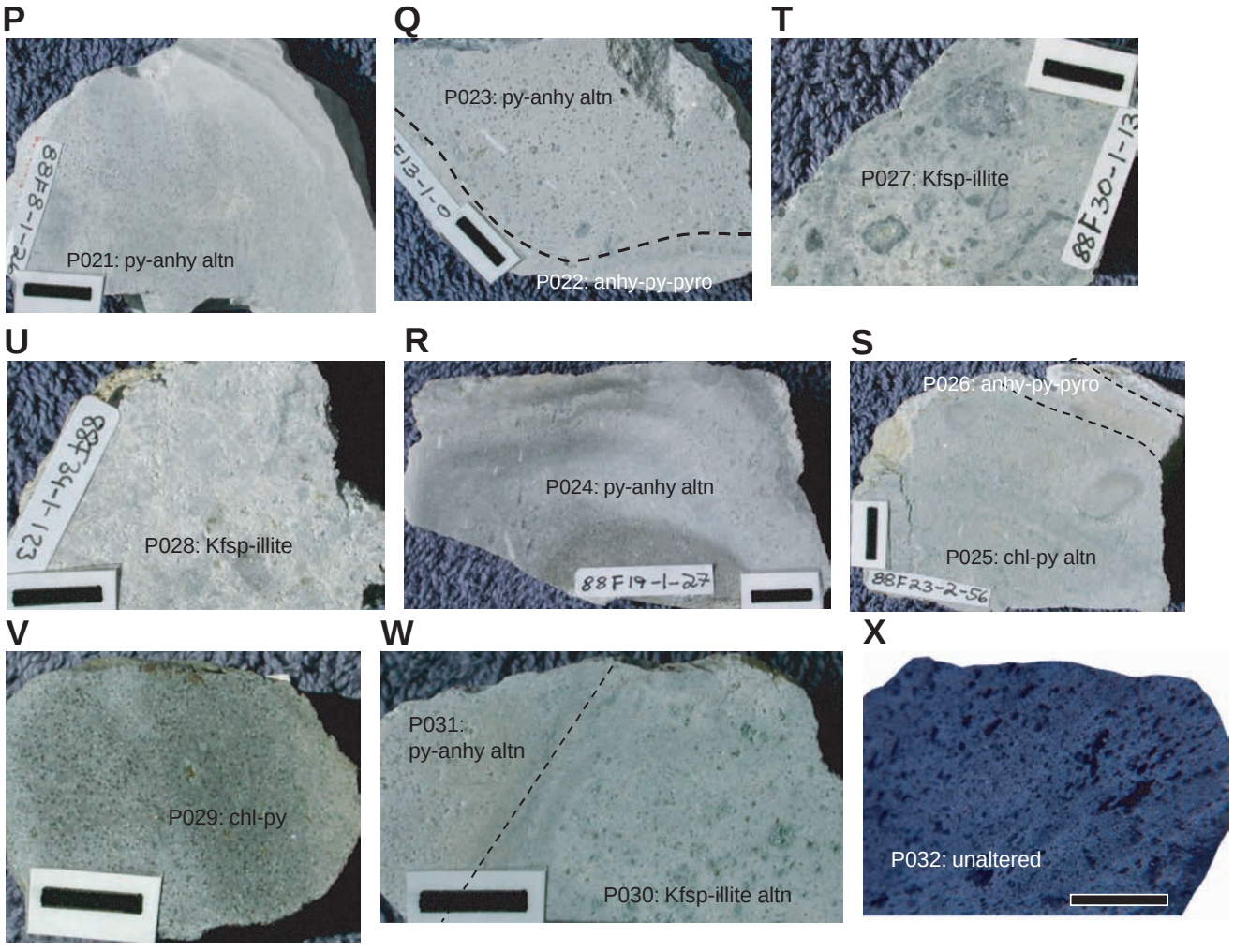

Figure F1 (continued). Y. Sample PM45 (193-1189A-2R-1, 0 cm): weakly altered ("dotted") aphyric coherent dacite. Bulk rock powder: P033 (XRF, ICP-MS, Cl, F, $\delta^{18}O_{silicate}$, $^{86}Sr/^{87}Sr_{silicate}$). **Z.** Sample PM47 (193-1189A-2R-1, 130 cm): perlitic dacite in anhydrite-rich stockwork zone. Powder of perlitic dacite separate (excluding anhydrite vein material): P034 (XRF, ICP-MS). **AA.** Sample PM48 (193-1189A-3R-1, 0 cm): vesicular coherent dacite. Bulk rock powder: P035 (XRF, ICP-MS, $\delta^{18}O_{silicate}$, $^{86}Sr/^{87}Sr_{silicate}$). **AB.** Sample PM49 (193-1189A-3R-1, 84 cm): vesicular coherent dacite. Bulk rock powder: P036 (XRF, ICP-MS, Cl, F, $\delta^{18}O_{silicate}$, $^{86}Sr/^{87}Sr_{silicate}$). **AC.** Sample PM50 (193-1189A-5R-1, 44 cm): domainal (white and green) altered, brecciated, flow-banded dacite. Powders of separates: P037 (green > white: XRF, ICP-MS, $\delta^{18}O_{anhydrite+silicate}$, $^{86}Sr/^{87}Sr_{anhydrite+silicate}$) and P038 (white > green: XRF, ICP-MS, $\delta^{18}O_{anhydrite+silicate}$, $^{86}Sr/^{87}Sr_{anhydrite+silicate}$). **AD.** Sample PM51 (193-1189A-7R-1, 11 cm): vesicular coherent dacite. Bulk rock powder: P039 (XRF, ICP-MS, Cl, F). **AE.** Sample PM52 (193-1189A-8R-1, 3 cm): coherent dacite. Bulk rock powder: P040 (XRF, ICP-MS, Cl, F). **AF.** Sample PM53 (193-1189A-9R-1, 21 cm): flow-banded, brecciated dacite. Bulk rock powder: 041 (XRF, ICP-MS, Cl, F, $\delta^{18}O_{anhydrite+silicate}$, $^{86}Sr/^{87}Sr_{anhydrite+silicate}$).

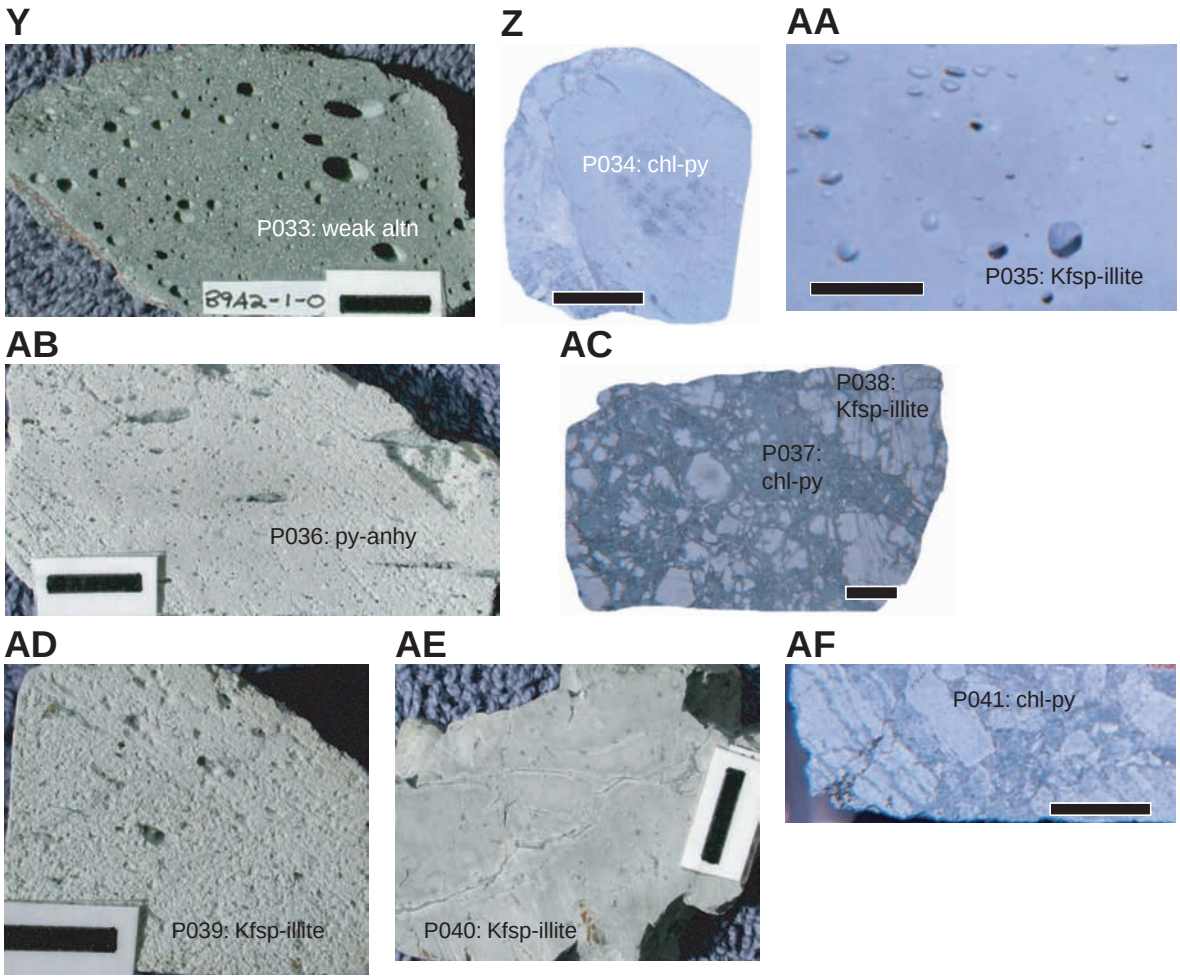

Figure F1 (continued). AG. Sample PM54 (193-1189A-10R-1, 39 cm): veined coherent dacite. Powders: P042 (coherent, unveined: XRF, ICP-MS, $\delta^{18}O_{silicate}$, $^{86}Sr/^{87}Sr_{silicate}$) and P043 (strongly veined: XRF, ICP-MS, Cl, F, $\delta^{18}O_{anhydrite+silicate}$, $^{86}Sr/^{87}Sr_{anhydrite+silicate}$). **AH.** Sample PM56 (193-1189A-12R-1, 83 cm): coherent dacite. Bulk rock powder: P044 (XRF, ICP-MS). **AI.** Sample PM57 (193-1189A-12R-1, 120 cm): mineralized pumice breccia. Powders of separates: P072 (pumice, illite-rich: ICP-MS) and P074 (sulfides: ICP-MS). **AJ.** Sample PM58 (193-1189A-13R-1, 51 cm): volcanic breccia. Bulk rock powder: P045 (XRF, ICP-MS, Cl, F, $\delta^{18}O_{silicate}$, $^{86}Sr/^{87}Sr_{silicate}$). **AK.** Sample PM60 (193-1189B-6R-1, 0 cm): perlitic dacite in jasper stockwork matrix. Powder of separates: P073 (dacite: XRF, ICP-MS) and P075 (jasper: ICP-MS). **AL.** Sample PM63 (193-1189B-11R-1, 22 cm): polymict volcanic breccia. Bulk rock powder: P046 (XRF, ICP-MS, Cl, F, $\delta^{18}O_{anhydrite+silicate}$, $^{86}Sr/^{87}Sr_{anhydrite+silicate}$). **AM.** Sample PM64 (193-1189B-11R-3, 3 cm): unaltered vesicular aphyric dacite. Bulk rock powder: P047 (XRF, ICP-MS, $\delta^{18}O_{silicate}$, $^{86}Sr/^{87}Sr_{silicate}$). **AN.** Sample PM68 (193-1189B-13R-1, 48 cm): perlitic coherent dacite. Bulk rock powder: P048 (XRF, ICP-MS, Cl, F, $\delta^{18}O_{silicate}$, $^{86}Sr/^{87}Sr_{silicate}$). **AO.** Sample PM71 (193-1189B-14R-1, 87 cm): flow-banded volcanic breccia. Bulk rock powder: P049 (XRF, ICP-MS, $\delta^{18}O_{anhydrite+silicate}$, $^{86}Sr/^{87}Sr_{anhydrite+silicate}$).

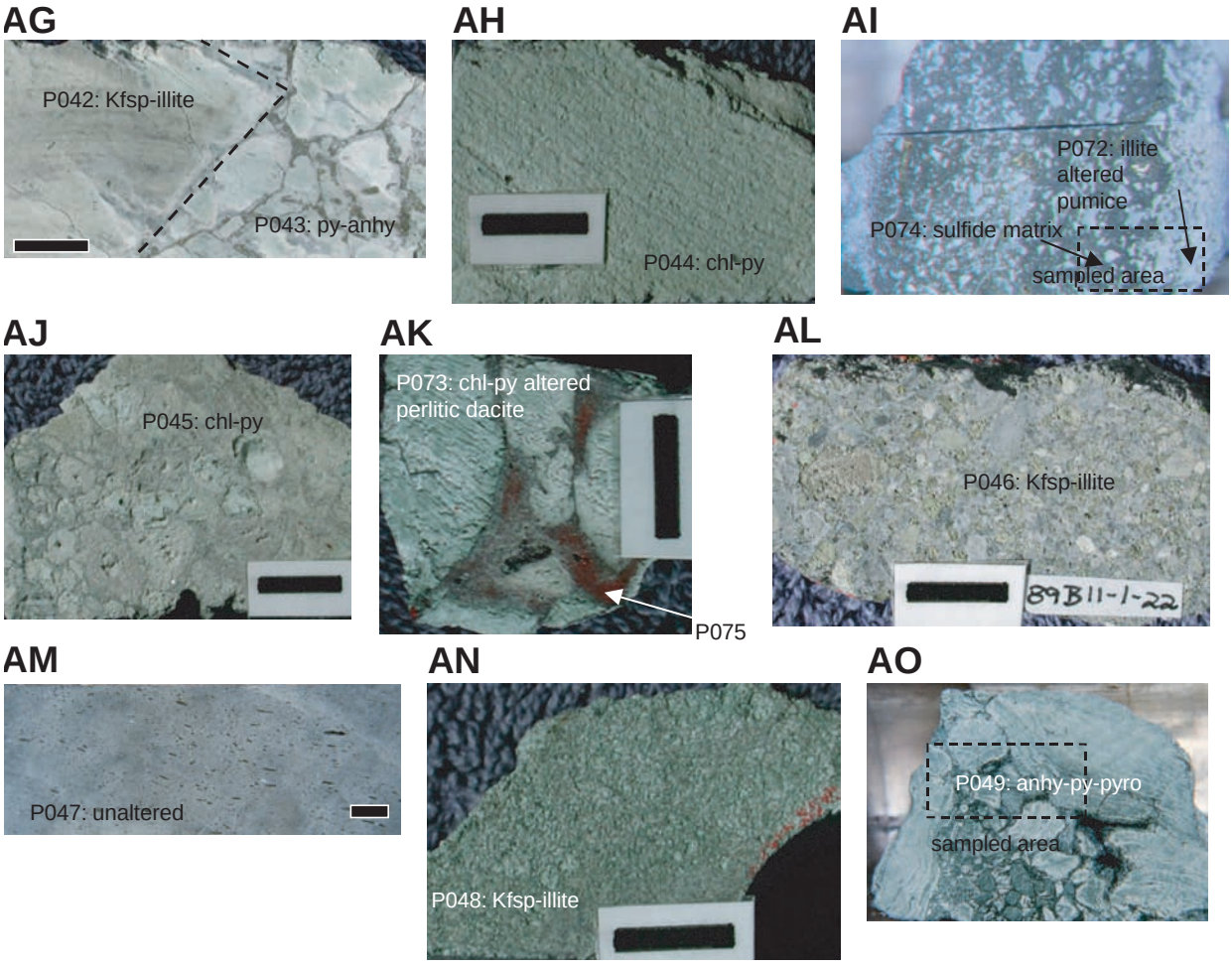

Figure F1 (continued). **AP.** Sample PM73 (193-1189B-15R-1, 25 cm): flow-banded volcanic breccia. Powders: P050 (clast: XRF, ICP-MS, $\delta^{18}O_{silicate}$, $^{86}Sr/^{87}Sr_{silicate}$) and P051 (matrix: XRF, ICP-MS, $\delta^{18}O_{silicate}$, $^{86}Sr/^{87}Sr_{silicate}$). **AQ.** Sample PM75 (193-1189B-15R-1, 124 cm): flow-banded volcanic breccia. Powders: P052 (gray clasts: XRF, ICP-MS, $\delta^{18}O_{silicate}$, $^{86}Sr/^{87}Sr_{silicate}$) and P053 (green clasts: XRF, ICP-MS, $\delta^{18}O_{silicate}$, $^{86}Sr/^{87}Sr_{silicate}$). **AR.** Sample PM79 (193-1189B-16R-1, 75 cm): weak, dotted alteration of vesicular coherent dacite. Bulk rock powder: P054 (XRF, ICP-MS). **AS.** Sample PM82 (193-1189B-17R-1, 57 cm): flow-banded coherent dacite. Bulk rock powder: P055 (XRF, ICP-MS). **AT.** Sample PM85 (193-1189B-18R-1, 5 cm): flow-banded volcanic breccia. Powder of separates: P056 (mainly gray clasts: XRF, ICP-MS) and P057 (mainly green matrix: XRF, ICP-MS). **AU.** Sample PM86 (193-1189B-18R-1, 45 cm): volcanic breccia with spherulitic clast. Powders: P058 (spherulitic clast: XRF, ICP-MS) and P059 (matrix: XRF, ICP-MS). **AV.** Sample PM88 (193-1189B-18R-1, 125 cm): volcanic breccia. Bulk rock powder: P060 (XRF, ICP-MS, Cl, F). **AW.** Sample PM89 (193-1189B-18R-2, 0 cm): flow-banded volcanic breccia. Bulk rock powder: P061 (XRF, ICP-MS, Cl, F).

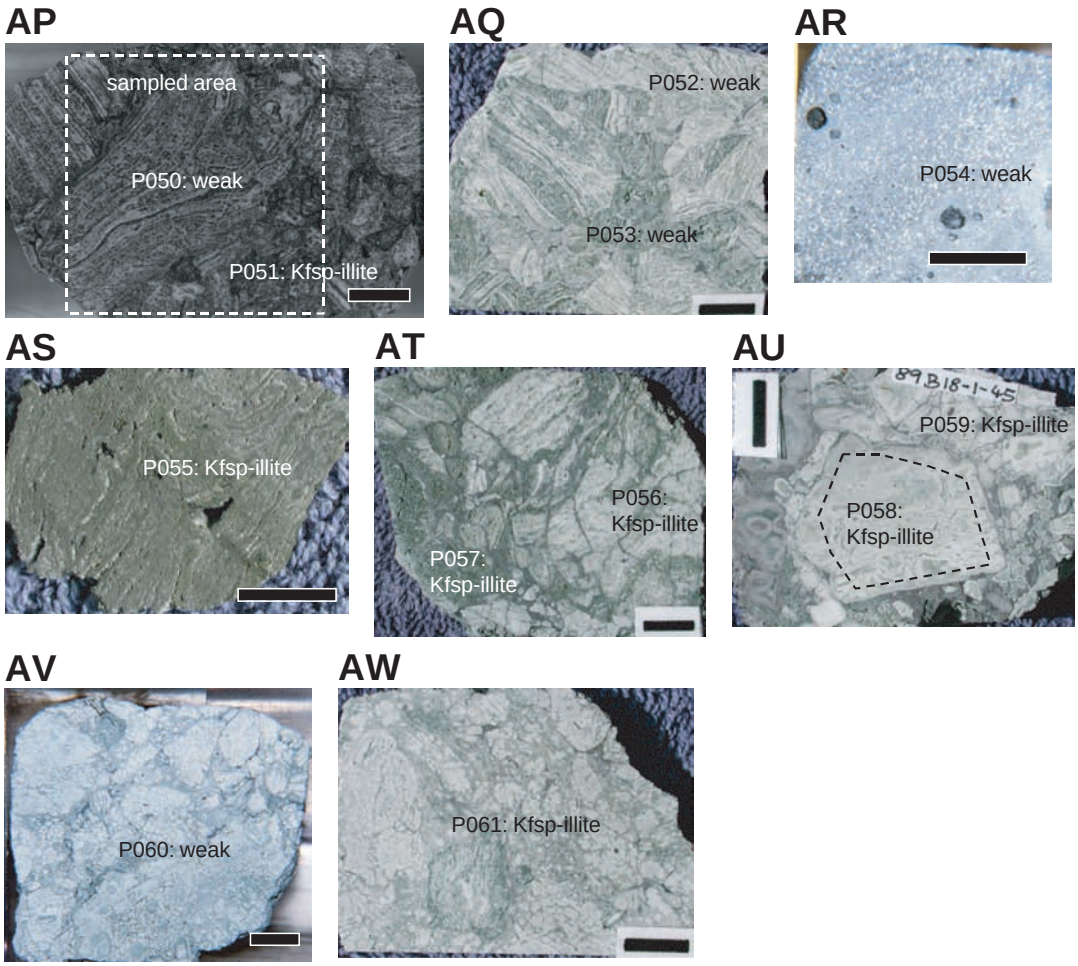

Figure F1 (continued). AX. Sample PM90 (193-1189B-18R-2, 49 cm): polymictic volcanic breccia. Powders: P062 (spherulitic clast: XRF, ICP-MS, $\delta^{18}O$, $^{86}Sr/^{87}Sr$), P063 (flow banded clast: XRF, ICP-MS, $\delta^{18}O_{silicate}$, $^{86}Sr/^{87}Sr_{silicate}$), and P064 (matrix: XRF, ICP-MS, $\delta^{18}O_{silicate}$, $^{86}Sr/^{87}Sr_{silicate}$). **AY.** Sample PM92 (193-1190C-3R-1, 3 cm): unaltered feldspar-phyric coherent dacite. Bulk rock powder: P065 (XRF, ICP-MS, $\delta^{18}O_{silicate}$, $^{86}Sr/^{87}Sr_{silicate}$). **AZ.** Sample PM93 (193-1191A-1R-1, 64 cm): unaltered, vesicular aphyric coherent dacite. Bulk rock powder: P066 (XRF, ICP-MS, Cl, F, $^{86}Sr/^{87}Sr_{silicate}$). Sample PM94 (193-1191A-1R-1, 75 cm): unaltered, vesicular aphyric coherent dacite. Bulk rock powder: P067 (XRF, ICP-MS, Cl, F, $\delta^{18}O_{silicate}$, $^{86}Sr/^{87}Sr_{silicate}$). Sample PM95 (193-1191A-3R-1, 80 cm): weak alteration of vesicular, aphyric coherent dacite. Bulk rock powder: P068 (XRF, ICP-MS, $\delta^{18}O_{silicate}$).

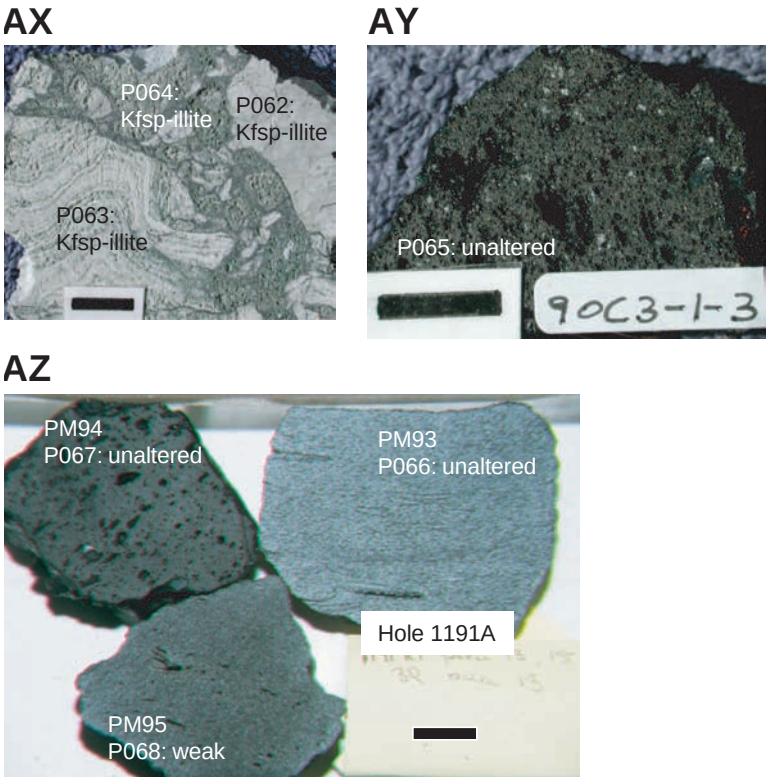

Figure F2. Based on differences in mineralogical and geochemical composition, several different types of alteration have been recognized. In these diagrams, the variable normative abundances of the most important minerals are illustrated, excluding SiO_2 polymorphs. The averages for pyrite and anhydrite are shown separately for each group of samples. Unaltered and weakly altered samples are rich in normative plagioclase and contain only traces of pyrite and anhydrite. Hydrothermal minerals such as chlorite, smectite, illite, and K-feldspar are abundant in chlorite-pyrite and K-feldspar-illite alterations. Anhydrite-pyrite-pyrophyllite alteration and pyrite-anhydrite alteration represent the most strongly altered samples, which contain no more primary plagioclase but abundant pyrite, anhydrite, illite, pyrophyllite, paragonite, and chlorite + smectite. There is considerable compositional variability within every group. (Continued on next page.)

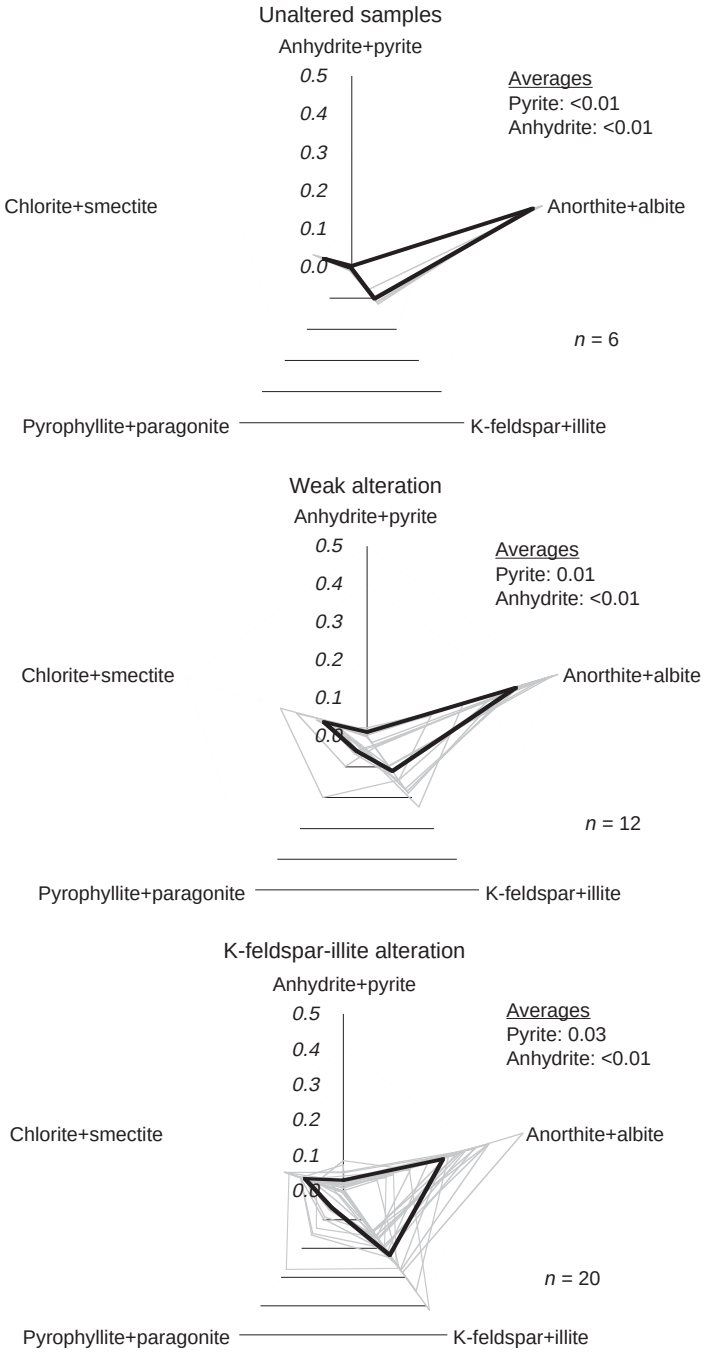

Figure F2 (continued).

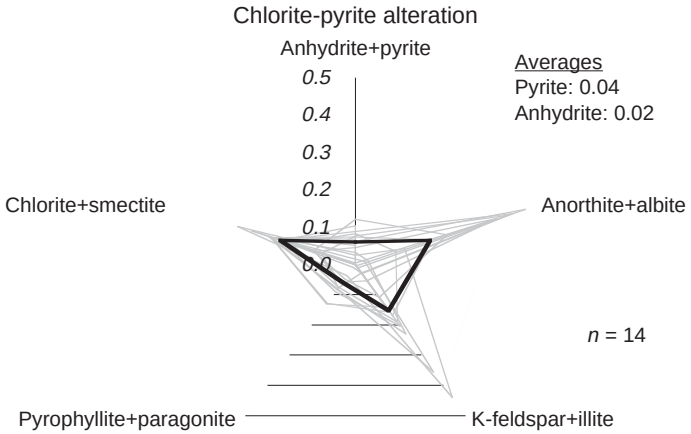

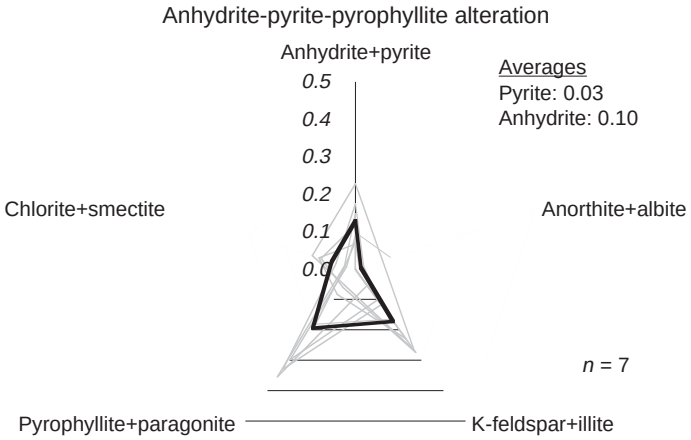

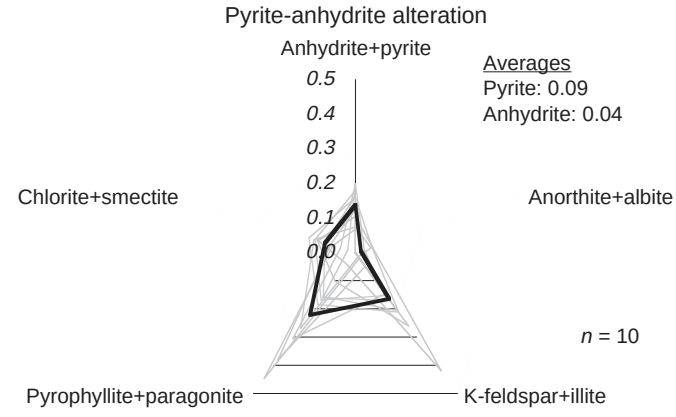

: Average of *n* analyses
: Individual analyses

Figure F3. The assemblages of hydrothermal minerals in altered dacite show systematic differences between the Snowcap and the Roman Ruins sites. At Roman Ruins there are abundant samples with high concentrations of normative K-feldspar, whereas at Snowcap the samples are comparatively poor in K-feldspar but contain elevated concentrations of pyrophyllite + paragonite.

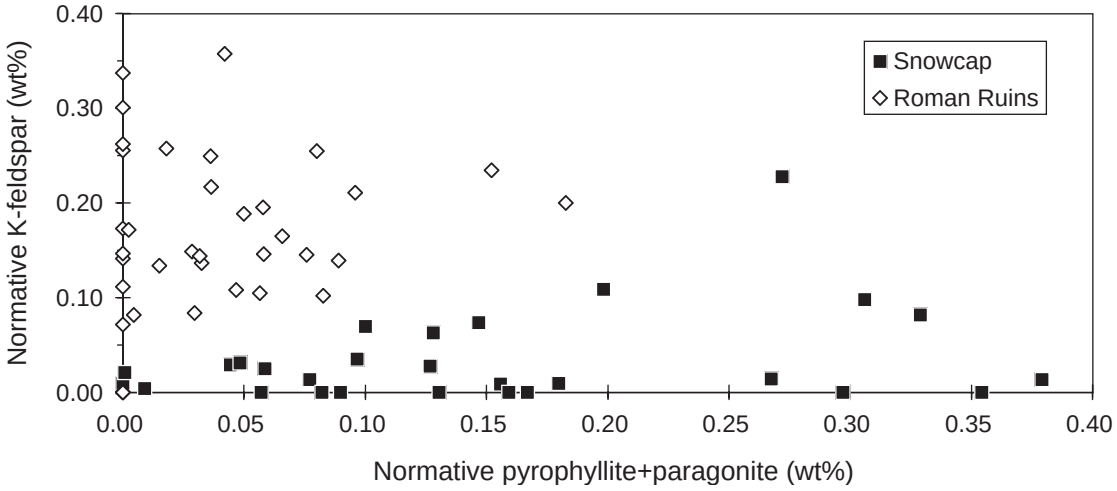

Table T1. Geochemistry of variably altered dacite from the PACMANUS hydrothermal field. (This table is available in an **oversized format.**)

Table T2. Results of XRD analysis. (This table is available in an **oversized format**.)